UNIVERSITY OF
BATH

University of Bath

1

Grace E. M. Lewis
Andrew J. Gross
Barbara Kasprzyk-Hordern
Anneke T. Lubben
Frank Marken

Department of Chemistry,
University of Bath, Bath, UK

Research Article

Feedback-amplified electrochemical dual-plate boron-doped diamond microtrench detector for flow injection analysis

An electrochemical flow cell with a boron-doped diamond dual-plate microtrench electrode has been developed and demonstrated for hydroquinone flow injection electroanalysis in phosphate buffer pH 7. Using the electrochemical generator-collector feedback detector improves the sensitivity by one order of magnitude (when compared to a single working electrode detector). The diffusion process is switched from an analyte consuming "external" process to an analyte regenerating "internal" process with benefits in selectivity and sensitivity.

1 Introduction

Generator-collector electrode systems have attracted attention in electroanalysis [1], exploiting the advantages of greater sensitivity (due to enhanced mass transport) and greater selectivity (due to additional dual potential control [2]). In particular novel nanogap generator-collector devices incorporated in flow systems are ground-breaking in terms of new analytical information obtained and improved sensitivity [3–5]. Dual-plate microtrench electrodes with down to 2 μm interelectrode gap [6, 7] have been introduced recently as a versatile and readily fabricated generator-collector electrode system with one open side to allow analyte diffusion into the interelectrode space (see Fig. 1).

The use of generator-collector electrode types in flow injection analysis is relatively common. Fenn et al. developed flow-through analytical cells with microgap generator-collector geometry [8] and amplification effects in twin-electrode cells were investigated for example by Anderson [9] and Yildiz [10]. Generator-collector flow analysis based on a dual-electrode device without amplification also are beneficial and powerful in analytical applications [11–13].

In this report, an electrochemical flow injection system is developed with a boron-doped diamond (BDD) dual-plate microtrench electrode as the detector. The BDD electrode in generator-collector mode has recently been demonstrated as a chemically robust electrode, for example for chloride determination at high potentials and with feedback amplification

in aqueous solutions [14]. Boron-doped diamond emerged as a very useful sp^3-carbon-type electrode material, most commonly in the form of thin films deposited on a suitable substrate or as a bulk poly-crystalline material [15]. BDD offers a wide potential window and the option to clean the electrode surface with aggressive cleaning reagents such as Piranha solution. BDD electrodes have been used analytically for the detection of pharmaceuticals [16] and for heavy metal determination [17].

Here, a simple flow injection system is employed with the BDD dual-plate detector in flow-through mode (with reference electrode upstream and counter electrode downstream). The schematic drawing in Fig. 1 shows the principle of operation and the flow geometry.

The two BDD electrodes are located opposite to each other with a 10 μm interelectrode distance with analyte flow over the top of the microtrench detector. Key parameters for the operation of the detector are (i) the inter-electrode distance δ, (ii) the trench length, and (iii) the trench depth. It is proposed that all three have a direct effect on the detector sensitivity in generator-collector operational mode.

2 Materials and methods

2.1 Reagents

Phosphate buffer solutions were prepared from H_3PO_4 and NaOH. Hydroquinone, hydrogen peroxide (20 wt.% in water), and sulphuric acid ($\geq$ 95–99%) were obtained from Sigma-Aldrich and used without further purification. Demineralized water was taken from a Thermo Scientific purification system (Barnstead Nanopure) with not less than 18 MΩ cm resistivity.

Correspondence: Dr. Frank Marken, Department of Chemistry, University of Bath, Bath BA2 7AY, UK
E-mail: F.Marken@bath.ca.uk

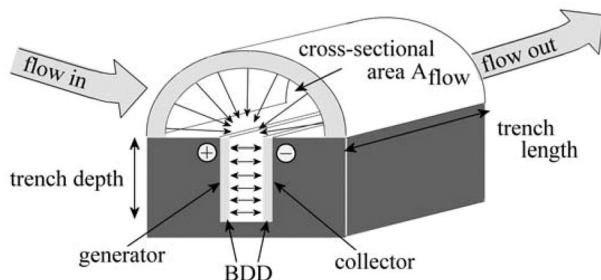**Abbreviation: BDD**, boron-doped diamond

Figure 1. Schematic drawing of the BDD dual-plate flow-cell trench detector with flow of analyte solution (with cross-sectional area A_{flow}) over the surface.

2.2 Instrumentation

A PGSTAT12 biopotentiostat system (Autolab, EcoChemie, The Netherlands) with GPES software was employed for generator-collector electrochemical measurements. The GPES software allows bipotentiostatic cyclic voltammetry or chronoamperometry experiments to be designed for paired electrode systems with simultaneous current read-out at both electrodes. A conventional four-electrode cell with a silver wire counter/reference electrode and a boron-doped diamond dual-plate microtrench working electrode was employed. All experiments were conducted at $22 \pm 2°C$.

2.3 Fabrication and calibration of boron-doped diamond dual-plate microtrench electrodes

Boron-doped diamond dual-plate micro-trench electrodes were fabricated using a literature method [14]. In brief, a single layer of SU-8-2002 was spin coated onto two separate 5×20 mm BDD substrates (300 nm BDD, SiO_2/Si_3N_4 interlayer, 8000 ppm doping and resistivity $= 10$ mΩ cm, purchased from NeoCoat SA, Switzerland), at 500 rpm for 15 s then 3000 rpm for 30s. Next, the two electrodes were pushed together, vis-à-vis, and placed onto a hot plate at 90°C (2 min) and the temperature was then ramped to 160°C and held for a further 5 min. After cooling to room temperature, the end of the dual-plate electrode was sliced off using a diamond cutter (Buehler, Isomet 1000 precision saw) and polished flat. Placing the electrode into Piranha solution (1:5 v/v H_2O_2:H_2SO_4; *Warning: Piranha solution is highly corrosive and appropriate precautions are needed*) etched the photoresist to form a microtrench electrode with dimensions of depth = 58 μm, length = 5 mm, and interelectrode gap, $δ = 10$ μm (see Fig. 2). After etching, the micro-trench electrode was cleaned with demineralized water and conducting copper tape (RS) was applied to give two electrode contacts.

In order to investigate the symmetry of the trench and to calibrate the depth of the trench the reduction of 1 mM $Ru(NH_3)_6^{3+}$ in 0.1 M KCl was employed (Fig. 3). In Fig. 3A voltammograms obtained with only one electrode connected to the potentiostat are shown. Although small differences in shape are apparent (mainly due to imperfections at the trench
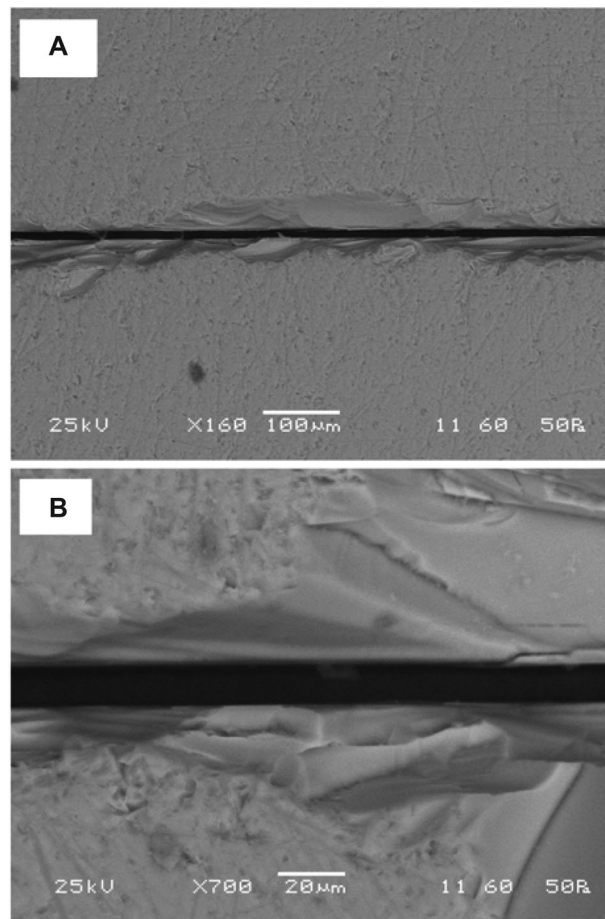

Figure 2. Scanning electron micrographs with (A) lower and (B) higher magnification showing the BDD generator-collector trench with a width of typically $δ = 10$ μm.

edge) between the two BDD electrodes (i and ii) the close similarity of these signals suggests a high quality symmetric dual-plate BDD electrode. Figure 3B and C show generator-collector feedback voltammograms with the collector held at 0.4 V versus SCE. The limiting current for mass transport controlled feedback is approximately $I_{lim} = 2.5$ μA.

The depth of the trench can be estimated based on the assumption of a symmetric (Nernstian [18]) concentration profile and approximately equal diffusion coefficients for the oxidised and reduced species ($D_{ox} = D_{red} = D = 0.9 \times 10^{-9}$ m^2 s^{-1}, the diffusion coefficient) [19].

$$\text{depth} = \frac{I_{lim} \times δ}{nFDc \times \text{length}} = 58 \text{ μm} \qquad (1)$$

In this equation, I_{lim} is the mass transport limited current, $δ$ is the inter-electrode gap of the microtrench as determined by electron microscopy, D is the diffusion coefficient, n is the number of electrons transferred per molecule diffusing to the electrode surface, F is the Faraday constant, c is the bulk concentration, and *length* is the overall length of the trench, here 5 mm. The estimated trench depth of 58 μm suggests an aspect ratio of ca. 6, which is consistent with previous reports for similar types of electrodes [20].
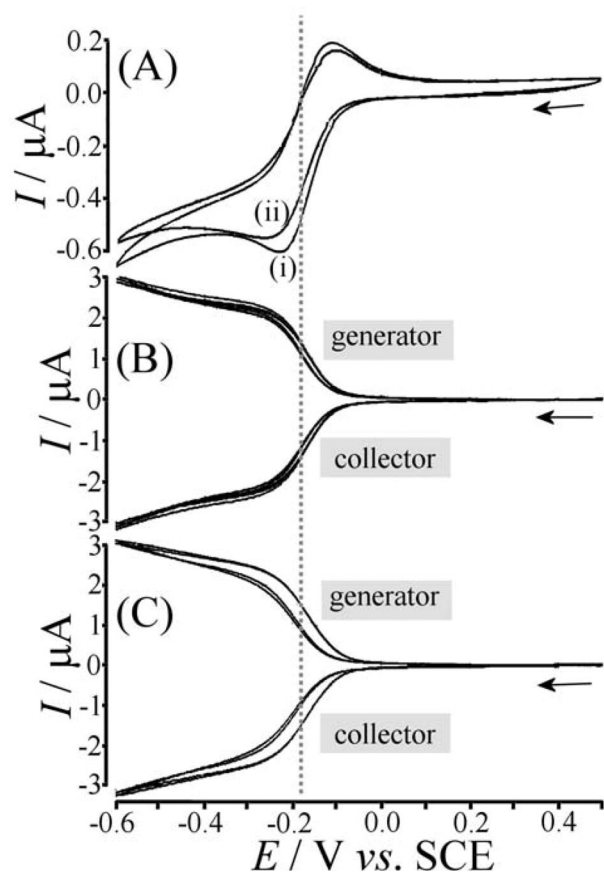
Figure 3. (A) Cyclic voltammograms (scan rate 20 mVs^{-1}) for the reduction of 1 mM Ru(NH$_3$)$_6$$^{3+}$ in 0.1 M KCl at a BDD dual-plate electrode with only electrode 1 (i) or only electrode 2 (ii) active. Voltammograms in (B) and (C) are recorded under the same conditions with electrode 2 or electrode 1, respectively, held at 0.4 V versus SCE in generator-collector mode.

2.4 Electrochemical flow analysis system

The electrochemical flow cell uses a 6-port 2-position switch valve to control the injection of the sample and a syringe pump (KD Scientific Model 781100, USA) to maintain the flow of the supporting electrolyte. The injection volume was 20 μL. The BDD dual-plate detector electrode was placed between a reference electrode (upstream) and a counter electrode (downstream) with flow over the trench as shown in Fig. 1.

3 Results and discussion

3.1 BDD dual-plate generator-collector voltammetry: hydroquinone oxidation under stagnant conditions

The oxidation of hydroquinone (see Eq. 2) is employed as a model redox system to explore the sensitivity of the BDD
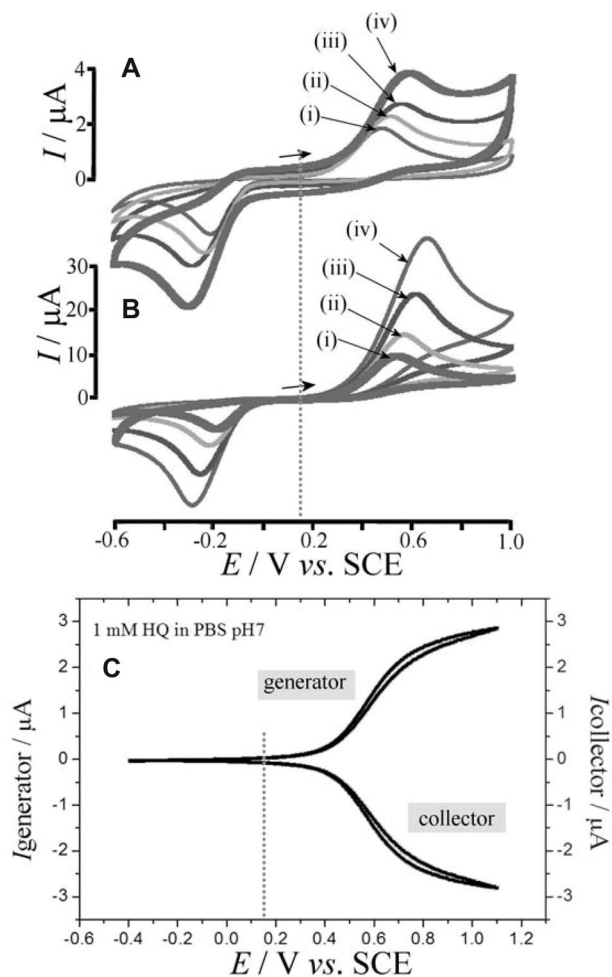

Figure 4. (A and B) Cyclic voltammograms (scan rates (i) 20, (ii) 50, (iii) 100, and (iv) 200 mVs^{-1}) obtained at boron-doped diamond electrodes (5 mm × 5 mm active area) in 0.1 M phosphate buffer pH 7 for the oxidation of (A) 0.1 mM hydroquinone and (B) 1 mM hydroquinone. (C) Generator-collector voltammograms (scan rate 20 mVs^{-1}, collector potential −0.4 V versus SCE) for the oxidation of 1 mM hydroquinone at a dual-plate BDD trench electrode immersed in 0.1 M phosphate buffer pH 7. The dotted line indicates the midpoint potential.

dual-plate microtrench detector for a classical electrochemically irreversible (but chemically reversible) test system [21].

(2)

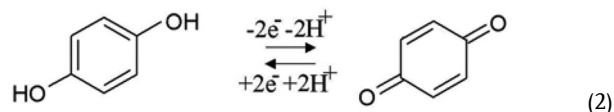Figure 4A and B show cyclic voltammograms recorded at various scan rates at a single 5 × 5 mm BDD working electrode for 0.1 and 1.0 mM hydroquinone, respectively. The wide peak-to-peak separation highlights the relatively slow rate of electron transfer at the diamond electrode consistent with literature reports [22]. The peak currents scale with the square root of scan rate and with the hydroquinone

concentration as anticipated for a diffusion-controlled peak. The midpoint potential $E_{mid} = \frac{1}{2}\,E_{ox} + \frac{1}{2}\,E_{red}$ is indicated by a dotted line at approximately 0.16 V versus SCE (in phosphate buffer pH 7 [22]).

The generator-collector voltammetric response for the oxidation of 1 mM hydroquinone (with the collector potential fixed at −0.4 V versus SCE) is shown in Fig. 4C. A well-defined feedback signal can be observed with a general increase in currents due to the feedback effect. The symmetry of generator and collector current suggest a well-defined redox cycle process with a shift in the current response away from the midpoint potential due to the irreversible nature of the electron transfer process. The mass transport controlled limiting current, approximately 2.8 μA, can be employed to determine the diffusion coefficient (Eq. 3).

$$D = \frac{I_{lim} \times \delta}{nFc \times length \times depth} = 0.5 \times 10^{-9}\,m^2 s^{-1} \qquad (3)$$

This value is reasonably consistent with literature values for the hydroquinone diffusion coefficient [23] and confirms that the process observed here is mass transport limited and in agreement with a feedback-amplified process.

3.2. BDD dual-plate generator-collector chronoamperometry I.: Hydroquinone oxidation under flow conditions without feedback

Next, the oxidation of hydroquinone in 0.1 M phosphate buffer pH 7 is studied by chronoamperometry using flow conditions with a BDD dual-plate micro-trench electrode configured as shown in Fig. 1. With the potential of one of the two BDD electrodes held at 1.0 V versus SCE and injection of hydroquinone (20 μL of a 1 mM solution), clear peak currents are observed (see Fig. 5A). The shape of peaks (in particular the width) is dependent on the flow rate of the analyte with peak broadening approximately proportional to flow speed. This observation is consistent with a process where the analyte in the reservoir over the trench electrode (see Fig. 1) is only partially consumed and diffusion toward the microtrench (like a microband) is dominating the detector current. The analyte present in the liquid phase is only partially consumed with a charge under the peak of typically 2.5 μC for a flow rate of 10 mL/h. For a 20 μL plug of liquid containing 1 mM hydroquinone complete consumption would result in a peak with 3.8 mC charge. Therefore only a very small fraction of the analyte can diffuse into the micro-trench under these conditions. From the peak duration (peak width at half height = 20 s at 2.7 μL/s) the flow cross-sectional area for the detector can be estimated as $A_{flow} = \frac{delay\ time \times flow\ velocity}{length} = 6.8\,mm^2$ where the delay time is the peak duration, 20 s, minus the theoretical peak duration for a very short detector, 7.4 s.

The effect of hydroquinone concentration is shown in Fig. 5B and C. Well-defined peak responses for 1 mM, 100 μM, and 10 μM hydroquinone are observed and a double logarithmic plot (Fig. 5D) shows linear dependence of hydroquinone concentration at 10 mL/h flow rate. The

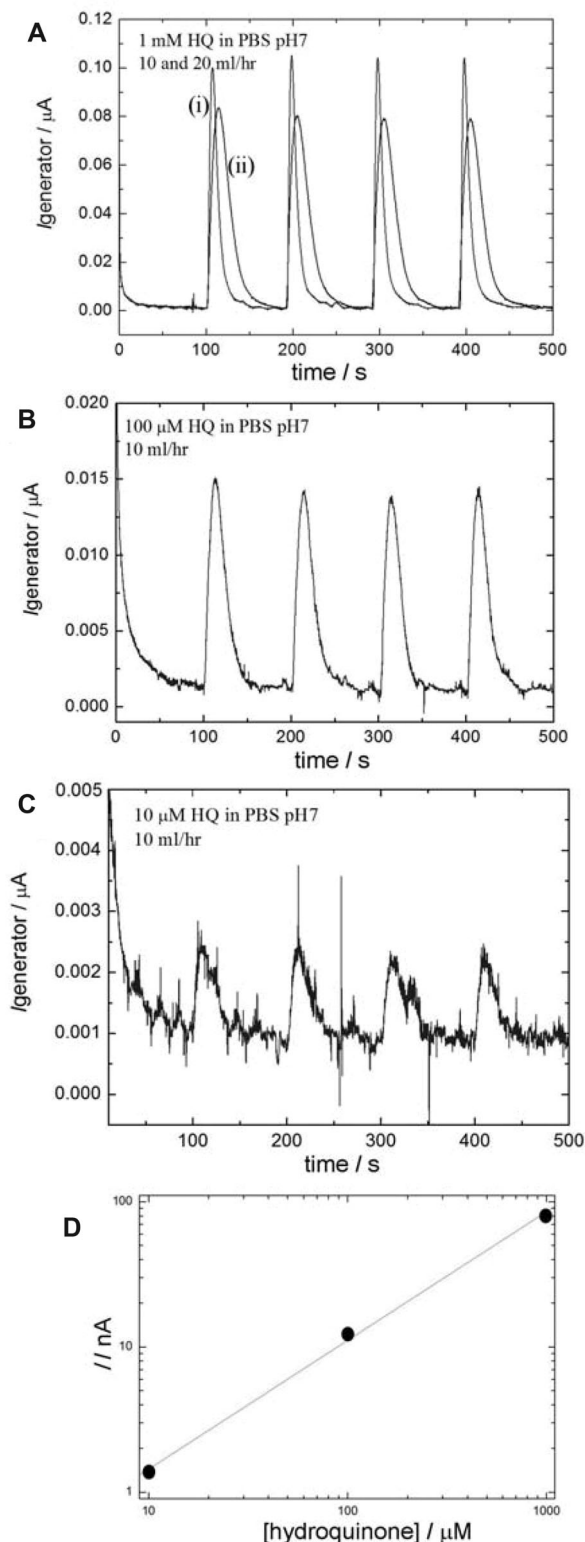**Figure 5.** (A) Flow-chronoamperometry data (applied potential 1 V versus SCE, flow rate (i) 20 mL and (ii) 10 mL/h) obtained at a BDD dual-plate electrode with only one electrode connected in 0.1 M phosphate buffer pH 7 for the oxidation of 1 mM hydroquinone. (B) As above but for 0.1 mM hydroquinone. (C) As above, but for 0.01 mM hydroquinone. (D) Double-logarithmic plot of peak current versus hydroquinone concentration.

low concentration range signal is limited by background noise. The maximum peak current under these conditions can be related to the current toward a microband (here the microtrench) as given in Eq. 4 [24–26].

$$I_{\text{peak,single-electrode}} = nFD \times length \times c$$

$$\times \left[\frac{\pi e^{-2.5\sqrt{\frac{\pi Dt}{\delta^2}}}}{4\sqrt{\frac{\pi Dt}{\delta^2}}} + \frac{\pi}{\ln\left(\left[\frac{64e^{-0.577}Dt}{\delta^2}\right]^{1/2} + e^{5/3}\right)} \right] \quad (4)$$

In this equation, n is the number of electrons transferred per molecule arriving in the trench, F is the Faraday constant, D is the diffusion coefficient for hydroquinone, *length* is the trench length, c is the (average) hydroquinone concentration, δ is the trench width, and t is the diffusion time. For a 10 mL/h flow rate the time between current onset and current peak is 4.4 s (see Fig. 5A), which allows a peak current to be predicted. The calculated value 0.33 μA is approximately four times higher compared to the observed peak current for 10 mL/h flow. The main reason for this deviation is likely to be some mixing in the space over the microtrench (see Fig. 1) lowering the apparent concentration (*vide infra*).

3.3. BDD dual-plate generator-collector chronoamperometry II.: Hydroquinone oxidation under flow conditions with feedback

With both electrodes active, the generator-collector system (i) allows amplification of the current signal and (ii) changes the operational mode into internal diffusion control (diffusion within the trench rather than diffusion toward the trench) without significant consumption of the analyte in the flow space. Fig. 6A shows current peak signals for 10 mL/h flow rate and with potentials applied to generator and collector of 1.0 V and −0.4 V versus SCE, respectively. The peak current is increased by an order of magnitude (compared to single electrode signals, see Fig. 5A–C) with peak width and shape remaining.

The magnitude of the peak current now is given by the internal mass transport which is approximately given by Eq. 5 [27].

$$I_{\text{peak,dual-electrode}} = \frac{nFD \times length \times depth \times c}{\delta} \quad (5)$$

The anticipated peak current is 2.8 μA (see Fig. 4C), which is approximately twice the experimental value (see Fig. 6A). This discrepancy is likely to be associated with the lower apparent concentration in the trench (as well as in the space over the trench) at the time of the peak due to non-ideal flow of analyte (no ideal plug flow and some degree of mixing in the space over the microtrench detector). Further evidence for this is obtained by changing the rate of flow. In Fig. 6B data for increased analyte flow rate are presented and the peak current can be seen to further decrease approximately inversely proportional to the flow rate. Therefore,
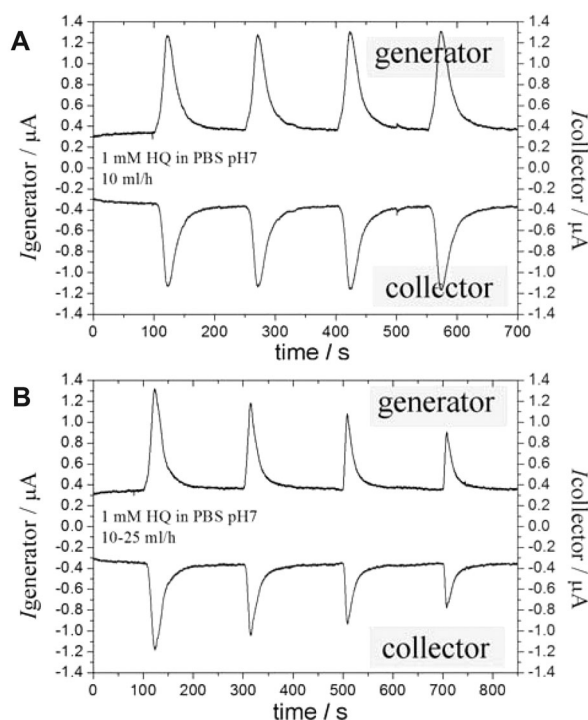

Figure 6. (A) Chronoamperometry data (applied generator potential 1 V versus SCE, applied collector potential −0.4 V versus SCE, flow rate 10 mL/h) obtained at a BDD dual-plate electrode with generator-collector feedback in 0.1 M phosphate buffer pH 7 for the oxidation of 1 mM hydroquinone. (B) As above but for a flow rate varying from 10 to 25 mL/h.

future improvements in the detector current signal are possible at lower flow rate and with more ideal flow geometry. Most importantly, even more significant improvements will be possible by (i) reducing the trench width δ, (ii) increasing the trench length (example.g., employing multiple parallel micro-trenches), and (iii) by increasing the trench depth.

4 Concluding remarks

A BDD dual-plate microtrench electrode detector has been successfully employed in an electrochemical flow injection cell. Proof-of-concept data by comparison of a single working electrode detector with a dual-electrode detector have been obtained. Although imperfections in the flow system currently limit the sensitivity, the generator-collector microtrench concept has been shown to be beneficial by switching the rate limiting diffusion process from outside to inside the microtrench of the BDD dual plate detector. With BDD offering a robust electrode material and Piranha etch cleaning allowing the detector performance to be maintained, this will be a useful new device when incorporated in chromatography or other separation techniques. Significantly lower LODs are anticipated for dual-plate electrodes where (i) the interelectrode distance δ is further decreased, (ii) the trench depth is increased, or (iii) the overall trench length is increased.

Very effective would be multi-trench devices where the total trench length is increased and more of the analyte solution can be sampled. Due to redox cycling within the microtrench, only insignificant fractions of the analyte are consumed. Further applications are possible where the generator-collector system is employed to suppress unwanted irreversible redox processes (e.g. oxygen reduction or ascorbate oxidation [20]), or to separate chemically irreversible analyte signals from chemically reversible redox processes.

The authors have declared no conflict of interest.

5   References

[1] Barnes, E. O., Lewis, G. E. M., Dale, S. E. C., Marken, F., Compton, R. G., *Analyst* 2012, *137*, 1068–1081.

[2] Honeychurch, K. C., Smith, G. C., Hart, J. P., *Anal. Chem.* 2006, *78*, 416–423.

[3] Mathwig, K., Lemay, S. G., *Electrochim. Acta* 2013, *112*, 943–949.

[4] Mathwig, K., Lemay, S. G., *Micromachines* 2013, *4*, 138–148.

[5] Lemay, S. G., Kang, S., Mathwig, K., Singh, P. S., *Acc. Chem. Res.* 2013, *46*, 369–377.

[6] Dale, S. E. C., Marken, F., in: Wadhawan, J. D., Compton, R. G., (Eds.) *Electrochemistry: Nanoelectrochemistry*, RSC, Cambridge 2014, pp. 132–154.

[7] Gross, A. J., Marken, F., *Electroanalysis* 2015, 10.1002/elan.201400554.

[8] Fenn, R. J., Siggia, S., Curran, D. J., *Anal. Chem.* 1978, *50*, 1067–1073.

[9] Anderson, L. B., Reilley, C. N., *J. Electroanal. Chem.* 1965, *10*, 295–296.

[10] Yildiz, A., Kissinger, P. T., Reilley, C. N., *Anal. Chem.* 1968, *40*, 1018–1019.

[11] Anderson, M. J., Crooks, R. M., *Anal. Chem.* 2014, *86*, 9962–9969.

[12] Amatore, C., Da Mota, N., Lemmer, C., Pebay, C., Sella, C., Thouin, L., *Anal. Chem.* 2008, *80*, 9483–9490.

[13] Amatore, C., Belotti, M., Chen, Y., Roy, E., Sella, C., Thouin, L., *J. Electroanal. Chem.* 2004, *573*, 333–343.

[14] Gross, A. J., Marken, F., *Electrochem. Commun.* 2014, *46*, 120–123.

[15] Compton, R. G., Foord, J. S., Marken, F., *Electroanalysis* 2003, *15*, 1349–1363.

[16] Einaga, Y., Foord, J. S., Swain, G. M., *MRS Bull.* 2014, *39*, 525–532.

[17] Jones, S. E. W., Compton, R. G., *Curr. Anal. Chem.* 2008, *4*, 170–176.

[18] Bard, A. J., Faulkner, L. R., *Electrochemical Methods* Wiley, New York, 2001, p. 29.

[19] Marken, F., Eklund, J. C., Compton, R. G., *J. Electroanal. Chem.* 1995, *395*, 335–339.

[20] Hasnat, M. A., Gross, A. J., Dale, S. E. C., Barnes, E. O., Compton, R. G., Marken, F., *Analyst* 2014, *139*, 569–575.

[21] Vuorema, A., Sillanpää, M., Rassaei, L., Wasbrough, M. J., Edler, K. J., Thielemans, W., Dale, S. E. C., Bending, S., Wolverson, D., Marken, F., *Electroanalysis* 2010, *22*, 619–624.

[22] Marken, F., Paddon, C. A., Asogan, D., *Electrochem. Commun.* 2002, *4*, 62–66.

[23] Adams, R. N., *Electrochemistry at Solid Electrodes*, Marcel Dekker, New York, 1969, p. 220.

[24] Lewis, G. E. M., Dale, S. E. C., Kasprzyk-Hordern, B., Lubben, A. T., Barnes, E. O., Compton, R. G., Marken, F., *Phys. Chem. Chem. Phys.* 2014, *16*, 18966–18973.

[25] Szabo, A., Cope, D. K., Tallman, D. E., Kovach, P. M., Wightman, R. M. *J. Electroanal. Chem.* 1987, *217*, 417.

[26] Amatore C., in Rubinstein, I., *Physical Electrochemistry*, Marcel Dekker, New York, 1995, p. 155.

[27] Dale, S. E. C., Vuorema, A., Sillanpää, M., Weber, J., Wain, A. J., Barnes, E. O., Compton, R. G., Marken, F., *Electrochim. Acta* 2014, *125*, 94–100.